ARTICLE

Boundary-Induced Auxiliary Features in Scattering-Type Near-Field Fourier Transform Infrared Spectroscopy

Jiong Yang,[†] Mohannad Mayyas,[†] Jianbo Tang,[†] Mohammad B. Ghasemian,[†] Honghua Yang,[‡] Kenji Watanabe,[§] Takashi Taniguchi,[§] Qingdong Ou,[∥] Lu Hua Li,[⊥] Qiaoliang Bao,[∥] and Kourosh Kalantar-Zadeh*,[†]

[†]School of Chemical Engineering, University of New South Wales (UNSW), Sydney Campus, NSW 2052 Australia
[‡]Bruker Nano, 112 Robin Hill Road, Santa Barbara, California 93117 United States
[§]National Institute for Materials Science, Namiki 1-1, Tsukuba, Ibaraki 305-0044, Japan
[∥]Department of Materials Science and Engineering, ARC Centre of Excellence in Future Low-Energy Electronics Technologies (FLEET), Monash University, Clayton, Victoria 3800 Australia
[⊥]Institute for Frontier Materials, Deakin University, Waurn Ponds, Victoria 3216 Australia

ⓢ *Supporting Information*

ABSTRACT: Phonon-polaritons (PhPs) in layered crystals, including hexagonal boron nitride (hBN), have been investigated by combined scattering-type scanning near-field optical microscopy (s-SNOM) and Fourier transform infrared (FTIR) spectroscopy. Nevertheless, many of such s-SNOM-based FTIR spectra features remain unexplored, especially those originated from the impact of boundaries. Here we observe real-space PhP propagations in thin-layer hBN sheets either supported or suspended by s-SNOM imaging. Then with a high-power broadband IR laser source, we identify two major peaks and multiple auxiliary peaks in the near-field amplitude spectra, obtained using scattering-type near-field FTIR spectroscopy, from both supported and suspended hBN. The major PhP propagation interference peak moves toward the major in-plane phonon peak when the IR illumination moves away from the hBN edge. Specific differences between the auxiliary peaks in the near-field amplitude spectra from supported and suspended hBN sheets are investigated regarding different boundary conditions, associated with edges and substrate interfaces. The outcomes may be explored in heterostructures for advanced nanophotonic applications.

KEYWORDS: *s-SNOM imaging, scattering-type nanoIR, hBN, phonon-polariton, near-field, boundary, nano-FTIR*
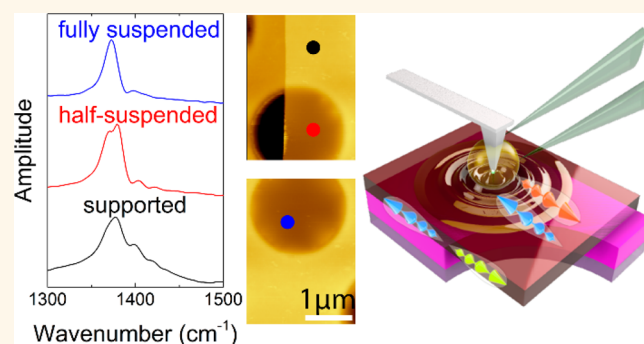
The combination of scattering-type scanning near-field optical microscopy (s-SNOM) and Fourier transform infrared (FTIR) spectroscopy has been demonstrated to generate spectra that are comparable to conventional FTIR spectra for the characterization of chemical components of organic materials.[1−5] Such combined s-SNOM and FTIR spectroscopy has also been shown as a sensitive tool for the nanoscale detection of strain and phase distribution in inorganic materials.[6−8] Logically, it is possible to spatially resolve the impact of boundaries using such a high spatial resolution spectroscopy across inorganic samples, as it provides sub-20 nm resolution.[1,9−11] However, there have been complexities in analyzing and extracting the information from spectra extracted using combined s-SNOM and FTIR

spectroscopy, in comparison to conventional FTIR spectra, for identifying such impacts. To date, due to the lack of powerful broadband IR laser sources and the resultant low signal-to-noise ratio near-field s-SNOM spectra, auxiliary peaks in such spectra have not been defined and their origins are still an open question. There is particular interest in near-field s-SNOM spectra in samples where polariton propagations are observed and influence the signals.[12−14] In such samples, the influence of boundaries on spectra has been observed,[15] but not analyzed. The boundaries can be edges or substrate
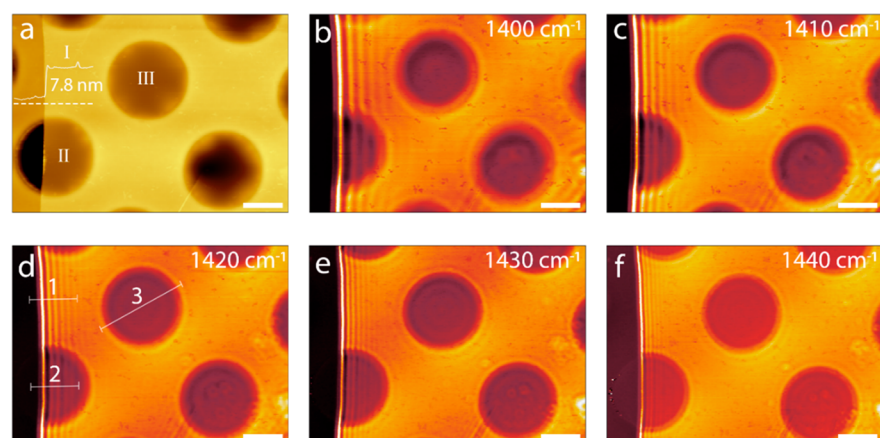
Figure 1. Real-space imaging of PhP propagation in the hBN crystal. (a) AFM image of the hBN sample consisting of supported and suspended areas. Regions I, II, and III denote the SiO_2-supported, the half-suspended, and the fully suspended regions, respectively. The hBN thickness was measured to be 7.8 nm along the white dashed line. (b−f) Near-field SNOM amplitude NF3 images of the hBN sample at illuminating frequencies of 1400 to 1440 cm^{-1}. Scale bar, 1 μm.

interfaces, and they can potentially have important effects on polariton behaviors.

In previous reports, spectra using combined s-SNOM and FTIR spectroscopy have been plotted into hyperspectral maps as a complementary method to s-SNOM imaging when studying phonon-polariton (PhP) dispersions.[12,15−19] The main hurdle to study such spectra has been the lack of access to powerful broadband IR laser sources to effectively couple with optical phonons, leading to the omittance of fine features. The femtosecond broadband laser used in our study (see Methods) provides >300 cm^{-1} spectral output at any given central wavenumber with a significantly large power. The laser power for the center wavenumber at around 1400 cm^{-1} used in our study is larger than 20 mW. As such, we were able to obtain extraordinarily high signal-to-noise ratio scattering-type near-field FTIR spectra with nanoscale spatial resolution (for brevity we term it as "scattering-type nanoIR") for a thin-layer hexagonal boron nitride (hBN) with a strong in-plane phonon peak near 1370 cm^{-1}. We also performed Gaussian peak fitting for scattering-type nanoIR amplitude spectra and discussed the origin of several groups of peaks.

We use hBN as the model inorganic material because its PhP propagation has been studied intensively as a stratified crystal.[16,20−25] PhPs in hBN can be launched by a nanoscale metal-coated probe[16,26] or by a local domain, where a giant dielectric change occurs.[19,21] It has been demonstrated that the isotopic variation[20] and the surrounding dielectric environment[19,27] can impact the PhP propagation in hBN, including its wavelength and propagation length. To study the effect of various boundaries on the PhP propagation, scattering-type nanoIR spectroscopy was utilized on a 7.8 nm hBN sheet that was mechanically exfoliated onto the 75 nm SiO_2/Si substrate with pre-etched microwells (Figure 1). The diameter of the microwells is approximately 2 μm.

RESULTS AND DISCUSSION

To begin with, we used the nanoIR3-s system (Bruker/Anasys) that was built on an atomic force microscope (AFM) to conduct s-SNOM imaging with a multichip quantum cascade laser (QCL, Daylight; see Methods). During the experiments, the QCL laser source was guided to the very fine apex of the AFM probe, which acts as a nanoantenna.[2,16,17,28] Figure 1a

shows the AFM image of the prepared hBN sample. In Figure 1a, it presents three typical regions marked by 'I', "II", and "III" as the SiO_2-supported, the half-suspended, and the fully suspended regions, respectively. Third-harmonic demodulation of the near-field amplitude signal (NF3) from s-SNOM imaging is shown in Figure 1b to f for illuminating frequencies of 1400 to 1440 cm^{-1}. PhP fringes can be clearly seen under different illuminating frequencies on all three regions. Within our measurement range in the upper Reststrahlen band, smaller illuminating frequencies result in sparser PhP fringes, indicating larger PhP wavelengths (λ_{PhP}).[16,18,29,30] This sample was specifically chosen to visualize multiple PhP fringes in the fully suspended region, which cannot be clearly resolved in thinner (1.3 nm, Figure S1 as an example) hBN sheets, consistent with previous reports.[16,31]

Along the three white lines marked as 1 to 3 in Figure 1d, line profiles were extracted, and they are presented in Figure 2a−c. The extracted data were averaged within the width of the white line. The black dotted line in Figure 2a and b denotes the edge of the hBN sheet. Both SiO_2-supported (Figure 2a) and half-suspended (Figure 2b) regions show similar fringe patterns that evolve with the illuminating frequency. Fringe patterns can also be observed in the fully suspended region, as shown in Figure 2c. The data points from the fully suspended region at illuminating frequencies of 1400 and 1410 cm^{-1} were not extracted because we did not observe enough full PhP propagation waves inside the fully suspended region. To better understand the launching mechanism of the PhP and the impact of the surrounding dielectric environment, a further data process was performed, and the results are presented in Figure 2d. The observed wavelength (λ_{obs}) of PhPs can be extracted by directly calculating the average distance between two adjacent peaks in the line profile in Figure 2a−c. The extracted λ_{obs} at different illuminating frequencies show interesting features. First, λ_{obs} of PhPs in the fully suspended region doubles that in the half-suspended region for each illuminating frequency from 1420 to 1450 cm^{-1}, indicating that PhPs in the fully suspended region were launched by the microwell boundary where large dielectric change occurred[19] and that λ_{obs} equals λ_{PhP} in this region. Second, λ_{obs} in the half-suspended region is always larger than that of the SiO_2-supported region, because of the change of the
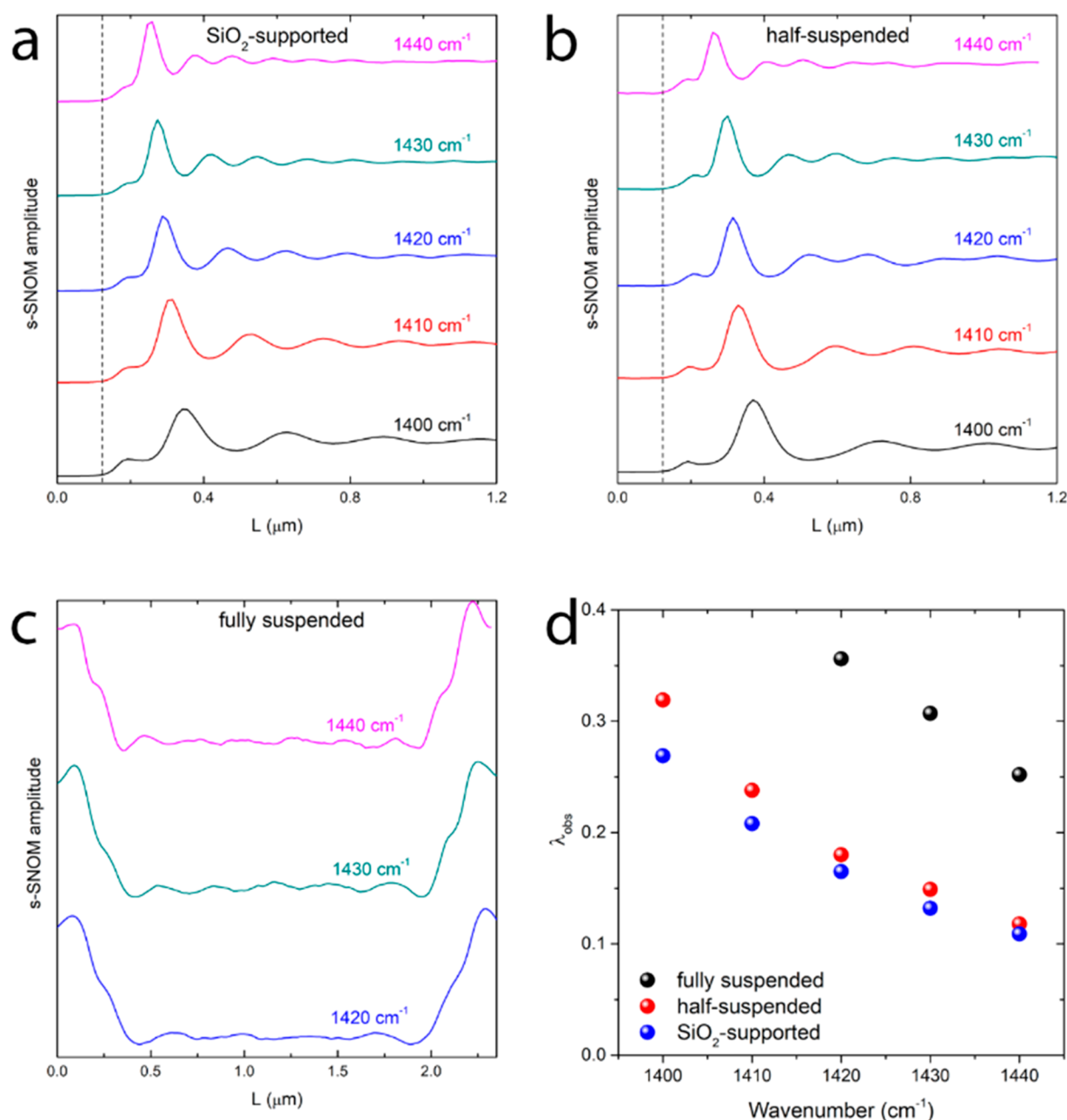
Figure 2. Evolution of the observed PhP wavelength (λ_{obs}) for hBN crystals under various dielectric environments. (a−c) Line profiles of near-field s-SNOM amplitude NF3 at different illuminating frequencies in (a) the SiO_2-supported, (b) the half-suspended, and (c) the fully suspended regions, along the white lines 1 to 3 in Figure 1d. (d) Extracted λ_{obs} of the fully suspended (black sphere), the half-suspended (red sphere), and the SiO_2-supported (blue sphere) region at different illuminating frequencies.

dielectric environment underneath the hBN crystal from SiO_2 to air.[27]

Afterward, we conducted scattering-type nanoIR spectroscopy with the same nanoIR3-s system on the exact sample with the QCL laser replaced by a high-power femtosecond broadband Camina laser (>20 mW in the experiment spectral output). We obtained near-field amplitude and phase spectra simultaneously (Figure 3) by using an asymmetric Michelson interferometer.[1,2,15] The spectral range was presented from 1300 to 1500 cm^{-1} to cover our s-SNOM imaging wavenumbers (with the actual measurement range from 1250 to 1550 cm^{-1} as one spectral output of the broadband laser, as shown in Figures S2−S5). To investigate the gradual spectral change under different boundary conditions, line scans with a

step size of 0.1 μm across different boundaries were carried out in our scattering-type nanoIR spectroscopy. The near-field signal was normalized to a Si substrate. It should be noted that our hBN sample remains stable under such high-power broadband IR laser irradiation, as can be seen from the AFM images in Figure S6 taken before and after the scattering-type nanoIR spectroscopy. The reason is that, at the wavenumber (wavelength) used in our experiment, the incident IR laser does not cause the deterioration of the hBN sample.

We show that our s-SNOM imaging and scattering-type nanoIR spectroscopy are self-consistent by plotting the near-field amplitude and phase spectra into hyperspectral maps,[16] as shown in Figure 4. PhP dispersions can be clearly observed in the SiO_2-supported and the suspended regions. In the
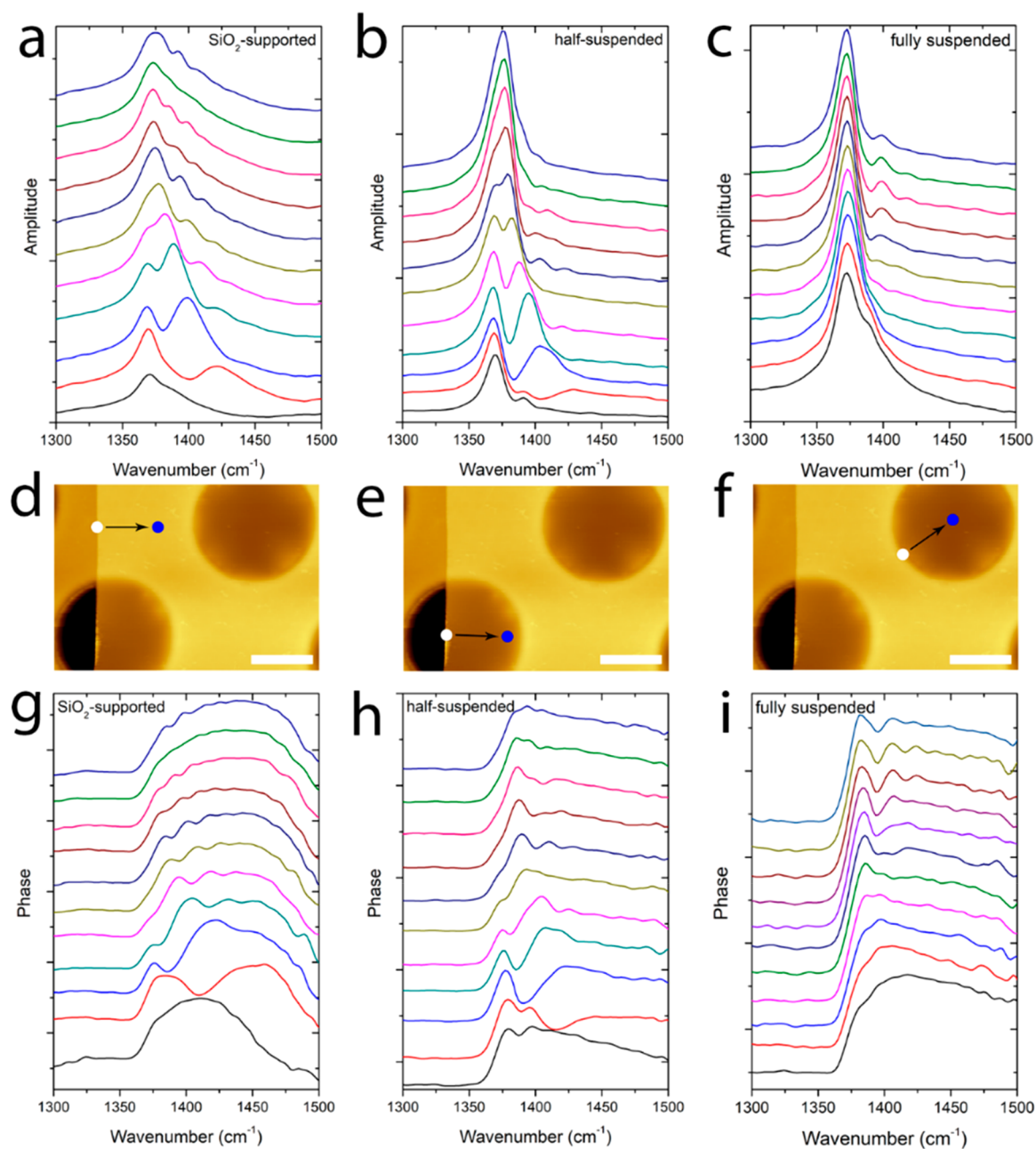
Figure 3. Evolution of the scattering-type nanoIR amplitude (a−c) and phase (g−i) spectra on the SiO₂-supported (a and g), half-suspended (b and h), and fully suspended (c and i) hBN. The spectra from bottom to top in each subfigure were taken from the starting point (white dots in d−f) to the ending point (blue dots in d−f) along the direction of the black arrows. Scale bar, 1 μm.

hyperspectral maps, the x-axis denotes the line-scan distance from the boundary inward, and the y-axis denotes the broadband laser wavenumber, with color indicating the amplitude intensity or phase change. In Figure 4a and c, hollow black triangles are extracted from single-frequency s-SNOM imaging data from Figure 1 in the corresponding area, and they follow the hyperbolic dispersion trend in the hyperspectral maps.

In the near-field amplitude spectra obtained from the SiO₂-supported (Figure 3a) and the half-suspended (Figure 3b) regions, we observed a major high-frequency peak approaching the main in-plane phonon peak near 1370 cm⁻¹ with the IR illumination moving from the hBN edge inward. Similar phenomenon can also be observed from the near-field phase spectra in Figure 3g and h. Near-field phase and amplitude

signals are Kramers−Kronig related.[15] Mathematically, the phase signal is the derivative of the amplitude signal. Previous reports[1,2] indicate that near-field spectral phase signals reflect the infrared absorption of organic materials. At this stage, we present both near-field amplitude and phase spectra and hope they can trigger further investigation. We will mainly discuss near-field amplitude spectra in this paper. We attribute the high-frequency major peak in Figure 3a and b to the interference between forward and backward PhP propagations,[15] and it vanishes when probed >0.6 μm away from the sample edge. This can also explain why we did not observe it in the fully suspended region (Figure 3c) as the whole line scan was far from the hBN edge. More interestingly, we observed a series of auxiliary peaks on the higher frequency side of those
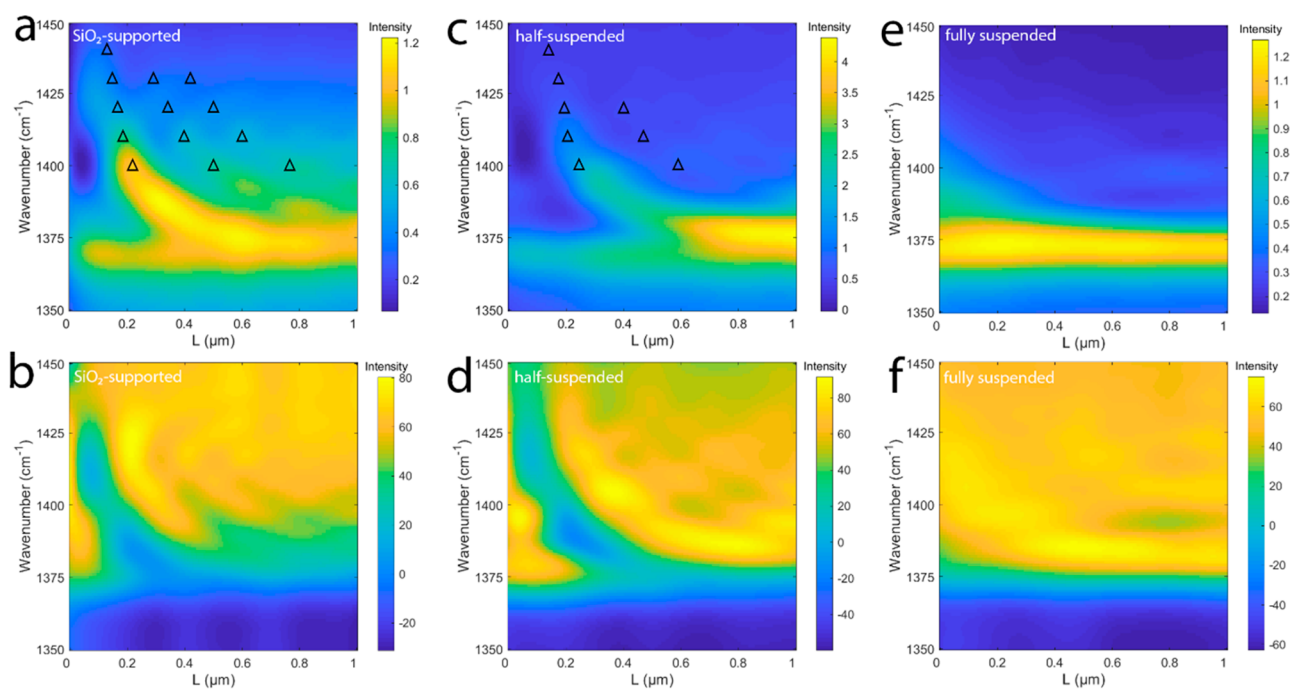
Figure 4. (a, b) Amplitude and phase PhP features as probed *via* line scans on the SiO$_2$-supported hBN. (c, d) Amplitude and phase PhP features as probed *via* line scans on the half-suspended hBN. (e, f) Amplitude and phase PhP features as probed *via* line scans on the fully suspended hBN. Black triangles in (a) and (c) are extracted from single-wavenumber s-SNOM imaging.

two major peaks when probing >0.2 μm away from the boundary. Such auxiliary peaks have never been identified.

By comparing Figure 3a and b, we found that the near-field amplitude spectrum probed at 1 μm away from the sample edge in the SiO$_2$-supported and the half-suspended regions differed from each other; the top spectrum in Figure 3a consists of one major peak and a series of auxiliary oscillations, while the auxiliary oscillations were less distinct in the half-suspended counterpart (with detailed peak intensity analysis presented in Figure S7). The difference of the SiO$_2$-supported region (Figure 3a) from the half-suspended region (Figure 3b) lies in the distance to the microwell edge and the presence of the SiO$_2$ layer. To reveal the origin of those auxiliary peaks, we conducted three sets of additional experiments.

First, we conducted scattering-type nanoIR spectroscopy on hBN supported by SiO$_2$ near the hBN edge but with different distances to the microwell edge (Figure 5) and near the microwell edge but far from the hBN edge (Figure 6). In Figure 5, near-field amplitude and phase spectra taken at the same distance from the hBN edge, but with different distances from the microwell edge, show certain interfering patterns for the auxiliary peaks, depending on the distances from the sample edge and the microwell edge, respectively. The presence of the shoulder in the higher frequency side of the spectra is seen when the IR illumination was moved closer to the microwell edge (Figure 5). The interfering patterns from these edges modulate the intensity of the spectral shoulders at different frequencies, depending on the distance from the edges. To realize the effect of the microwell edge without the impact from the hBN edge, near-field amplitude and phase spectra at different distances from the microwell edge, while very far from the hBN edge, were taken and shown in Figure 6. They all present similar spectral shoulders on the higher wavenumber side of the near-field amplitude spectra in addition to the main in-plane phonon peak. However, we

cannot observe the presence of some of the strong interfering PhP modulating peaks.

Second, we compared the near-field amplitude and phase spectra taken from partly suspended regions with different hBN coverages on the microwell, and the results are presented in Figure S8. Figure S8a and b show the near-field amplitude and phase spectra of the half-suspended hBN; Figure S8d and e show the near-field amplitude and phase spectra of the nearly quarterly suspended hBN. For comparison, the line-scan width was chosen to be 0.7 μm. Compared to the near-field amplitude spectra taken from the half-suspended region (Figure S8a), their counterparts taken from the quarterly suspended region show stronger auxiliary features (Figure S8d), indicating stronger interference between the hBN sample edge and the microwell edge due to the shorter distance between them.

Third, we prepared SiO$_2$-supported hBN samples on a 300 nm SiO$_2$/Si substrate with a thickness of 10.5 nm (comparable to 7.8 nm in thickness) and 28.6 nm (much larger than 7.8 nm in thickness). As can be seen in Figure S9a, the auxiliary peaks in the near-field amplitude spectra of the 10.5 nm hBN are significantly reduced in magnitude compared to Figure 3a. The near-field amplitude spectra are also obtained for the 28.6 nm hBN on 300 nm SiO$_2$ (Figure S9b), which show very similar reduced intensity auxiliary peaks to the 10.5 nm sample in terms of magnitude. To this point, the thickness of SiO$_2$ seems to play a more important role in amplifying the intensity of the auxiliary peaks by the resonance effect than the thickness of the hBN itself, which governs the distance from the near-field source at the apex of the AFM probe.[2,28,32]

The effect of hBN boundaries as a function of the hBN thickness can be considered independently. One important effect of the increase in the thickness of the hBN layer is the shift of the major in-plane phonon peak. This peak is centered at ~1370 cm^{-1} when the thickness of the layer is ~10 nm
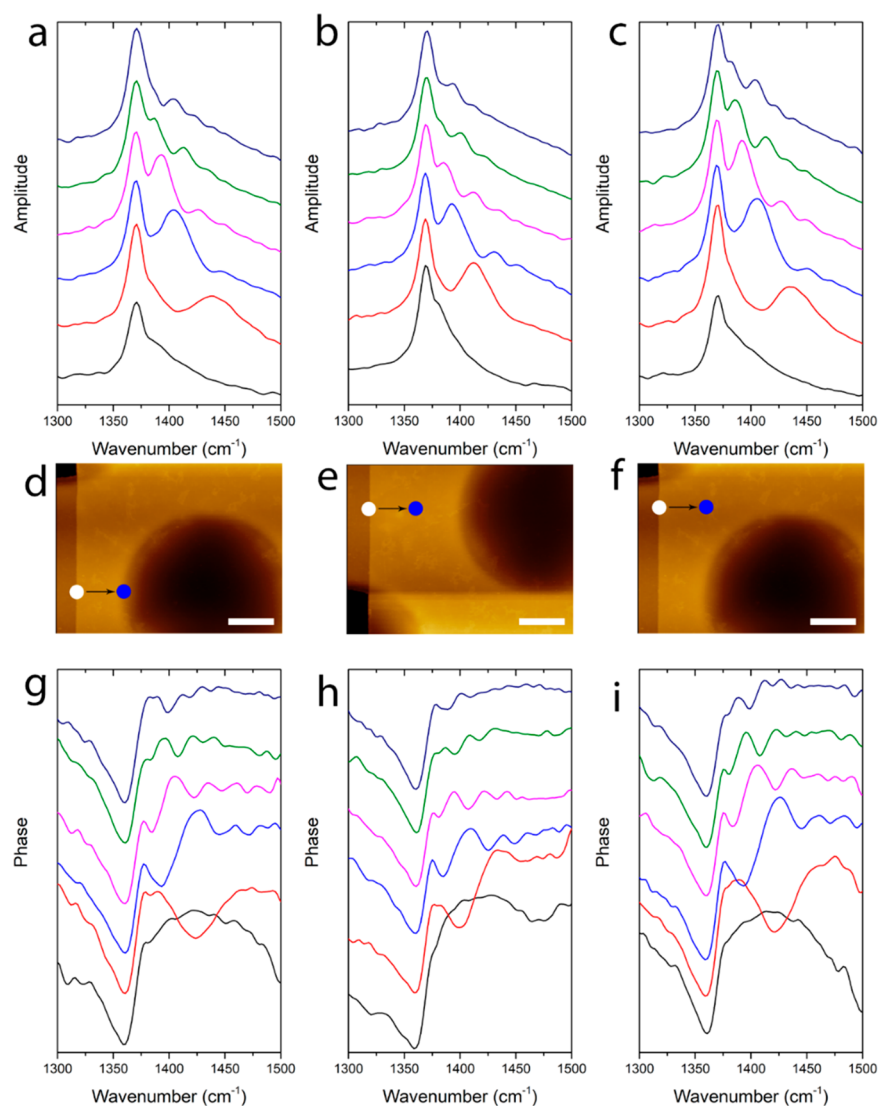
Figure 5. Evolution of the near-field amplitude (a−c) and phase (g−i) of hBN supported by SiO₂ but with different distances from the microwell edge. The spectra from bottom to top in each subfigure were taken from the starting point (white dots in d−f) to the ending point (blue dots in d− f) along the direction of the black arrows. Scale bar, 0.5 μm.

(Figure S9a) and it shifts up to ∼1380 cm^{-1} when the thickness increases to ∼30 nm (Figure S9b). It is known that this in-plane phonon peak shifts back to ∼1370 cm^{-1} when the hBN thickness increases to 75 nm or more.[15] However, no specific behavior in the formation of auxiliary peaks is observed in such hBN thickness changes.

Taking the experimental findings together, one can conclude that the thickness of the SiO₂ layer under hBN plays an important role in formation of auxiliary peaks in the near-field amplitude spectra, and the impact from the microwell edge should also be considered. Therefore, we attribute the multiple auxiliary oscillations from the SiO₂-supported hBN to PhP resonance emergence as a result of energy confinement within the 75 nm SiO₂ layer,[33−35] as depicted in Figure S10. Additionally, the weak auxiliary peaks in the half-suspended region can be assigned to the interference between the hBN edge and the microwell edge. The auxiliary peaks from the fully suspended hBN will be discussed later.

We found that Gaussian fitting can perfectly fit all the near-field amplitude spectra (with detailed fitting results shown in Figures S2 to S5). We were able to identity several groups of

peaks after peak fitting of spectra taken from the SiO₂-supported, the half-suspended, and the fully suspended regions, and the extracted peak center positions for those regions are plotted in Figure 7.

Based on the Gaussian function, an empirical formula was generated for our near-field amplitude spectra as follows:

$$\text{Amplitude} = A + \sum_{B_i, L_{ci}, \omega_i} B_i \frac{e^{-4\ln2\left(\frac{L-L_{ci}}{\omega_i}\right)^2}}{\omega_i} \qquad (1)$$

where A and B_i are constants, ω_i defines the full-width-at-half-maximum (fwhm) of the peaks, L is the distance to the sample boundary, and L_{ci} is the center location of the fitted peaks. Human intervention was minimized during fitting by choosing the starting point of the peak center location only where a peak or peak shoulder can be observed.

Furthermore, to simplify the question, we found that we could fit L_{ci} ($i > 2$) as a reciprocal function of L for the SiO₂-supported and the half-suspended region.
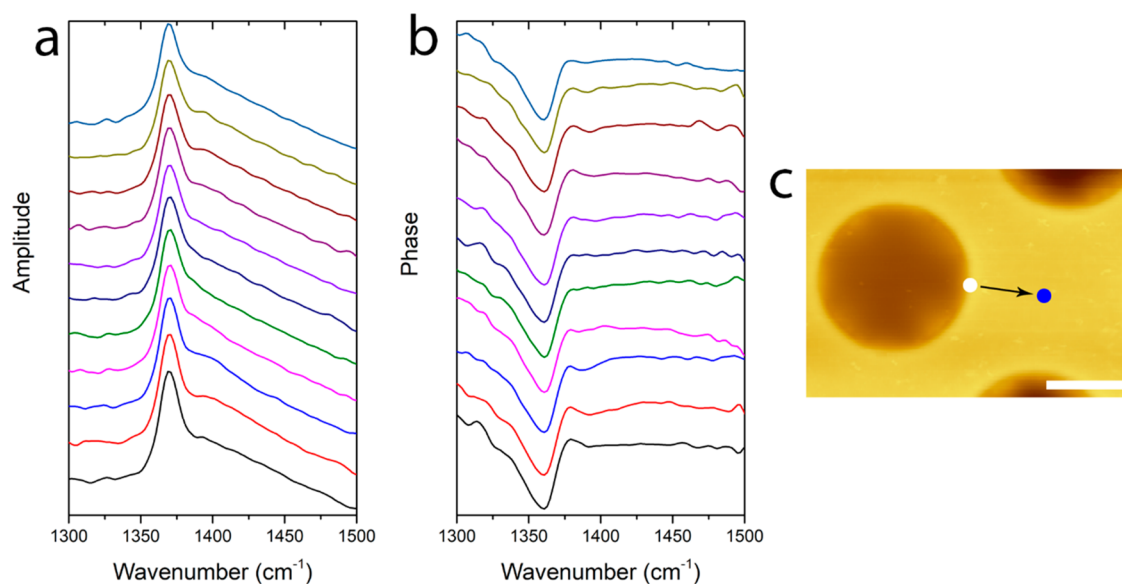
Figure 6. Evolution of the near-field amplitude (a) and phase (b) of hBN supported by SiO$_2$ near the microwell edge and far from the hBN edge. The spectra from bottom to top in each subfigure were taken from the starting point (white dots in c) to the ending point (blue dots in c) along the direction of the black arrows. Scale bar, 1 μm.
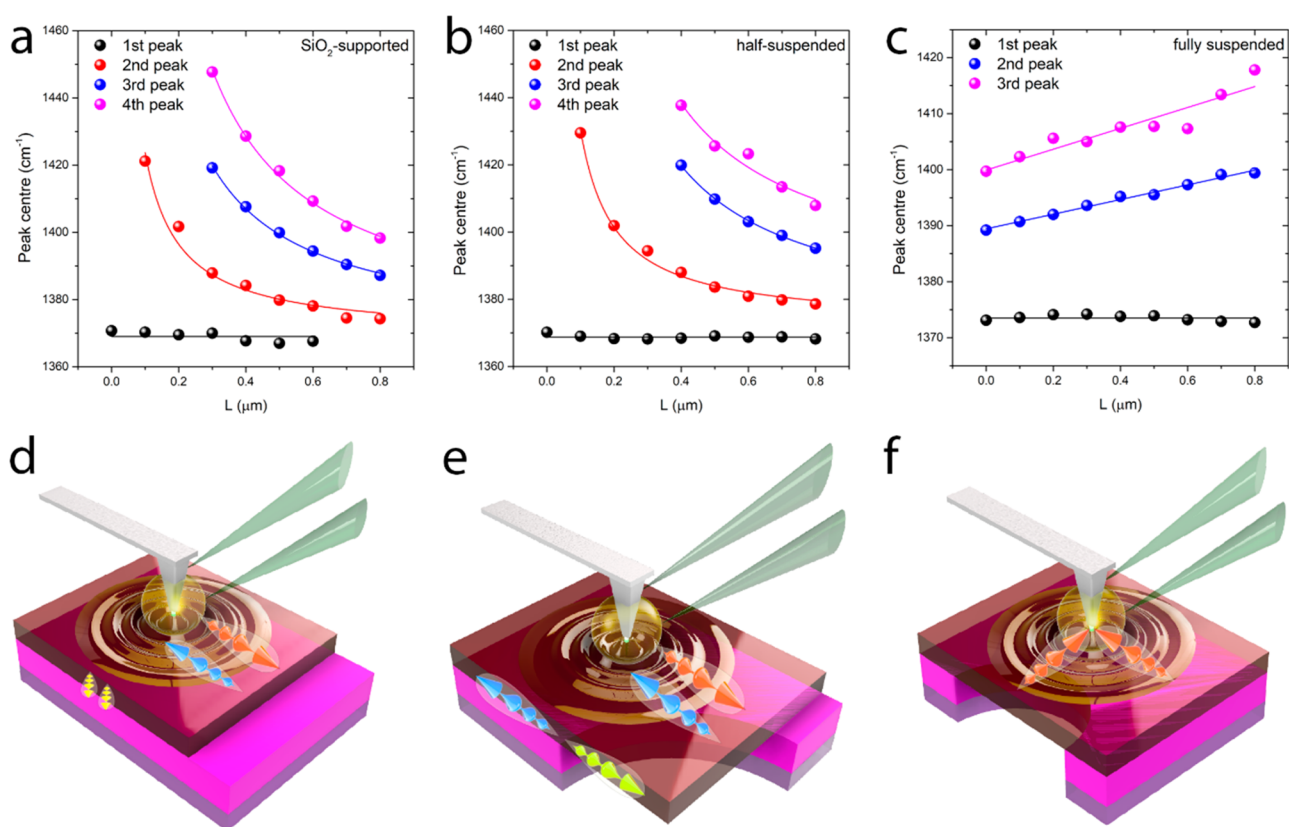

Figure 7. Peak-fitting results for near-field amplitude spectra from scattering-type nanoIR spectroscopy. (a–c) Fitted peak center positions for the 75 nm SiO$_2$-supported, the half-suspended, and the fully suspended regions, respectively. (d–f) Schematics of PhP propagations and interactions with boundaries in the (d) SiO$_2$-supported, (e) half-suspended, and (f) fully suspended regions.

$$L_{ci} = -m_i - \frac{n_i}{L} \qquad (2)$$

as shown by the solid curve in Figure 7a and b, where m_i and n_i are constants. But for the fully suspended region, we found that L_{ci} ($i > 2$) followed a linear relationship with L.

$$L_{ci} = -p_i - q_i L \qquad (3)$$

as shown by the solid curve in Figure 7c, where p_i and q_i are constants.

By combining the above eq 1 and eq 2, we can get that, for PhPs launched by the AFM probe and reflected by the hBN edge, the near-field amplitude spectra can be expressed by

$$\text{Amplitude} = A + \sum_{B_i, \omega_i, m_i, n_i} B_i \frac{e^{-4\ln 2 \left(\frac{m_i + L + \frac{n_i}{L}}{\omega_i} \right)^2}}{\omega_i} \tag{4}$$

By combining the above eq 1 and eq 3, we can get that, for PhPs launched by the microwell boundary, the near-field amplitude spectra can be expressed by

$$\text{Amplitude} = A + \sum_{B_i, \omega_i, p_i, q_i} B_i \frac{e^{-4\ln 2 \left(\frac{p_i + (q_i+1)L}{\omega_i} \right)^2}}{\omega_i} \tag{5}$$

It should be noted that eqs 4 and 5 only consider the three or four groups of peaks extracted from the near-field amplitude spectra.

In Figure 7a and b, black and red spheres denote the position of the in-plane phonon and the PhP propagation interference peaks, respectively. We have also successfully extracted two groups of auxiliary peaks from all three regions, as shown by blue and magenta spheres in Figure 7. As discussed previously, the auxiliary peaks in the near-field amplitude spectra from the SiO_2-supported region can be attributed to the resonance effect and confinement of the in-plane propagating energy within the 75 nm SiO_2 layer, as well as the weak interference between the hBN edge and the microwell edge, as illustrated in Figure 7d and e, respectively. By comparing Figure 7b with c, one can see that near-field spectral auxiliary peaks in the fully suspended region behave differently compared to those in the half-suspended region. In the half-suspended region, the auxiliary peaks move reciprocally toward the main in-plane phonon peak by following the PhP hyperbolic dispersion trend when the IR illumination moves away from the hBN edge. However, in the fully suspended region, two groups of auxiliary peaks move linearly away from the in-plane phonon peak when the IR illumination moves away from the microwell edge. This can be explained by the PhP resonating inside the fully suspended area,[12] as shown by the schematic in Figure 7f. After peak-fitting of additional near-field amplitude spectra, when scanning across the fully suspended region and extracting the peak center locations, we found that both groups of auxiliary peaks approach the in-plane phonon mode after scanning over the microwell, as presented in Figure S11. According to our experimental findings, the center of the microwell seems to be a smooth turning point for the auxiliary peak location.

CONCLUSIONS

In summary, we have conducted self-consistent s-SNOM imaging and scattering-type nanoIR spectroscopy on a 7.8 nm hBN sheet that experiences different boundary conditions. We observed PhP fringes in hBN either suspended or supported by the 75 nm SiO_2/Si substrate. With a high-power broadband IR laser source, we were able to resolve multiple groups of auxiliary peaks in the near-field amplitude spectra. We realized that the hBN edge produced one distinct major peak that moves toward the in-plane phonon peak and merges with it when the IR illumination exceeded the 0.6 μm distance from the edge. The strong resonance-related peaks were seen when the SiO_2 layer underneath was 75 nm thick, while they were mostly suppressed at 300 nm. We observed and identified the differences between the near-field auxiliary signatures when the hBN layers were supported or suspended, which are attributed to the interference between the microwell edge and the hBN

edge, depending on the distances from the edges. The appearance of the extra auxiliary peaks is an important observation that has been previously overlooked and can be used for defining localized boundary conditions and the resonance effect. Having such observations, these localized boundaries can be engineered for creating sensing and modulating nanophotonics.

METHODS

A commercial Bruker/Anasys AFM-based nanoIR3-s system was used to conduct both s-SNOM imaging and scattering-type nanoIR spectroscopy to study PhPs in the hBN sample. The AFM operates in tapping mode in both s-SNOM imaging and scattering-type nanoIR spectroscopy. The AFM probes (Bruker) used in this study are coated with conductive platinum silicide (PtSi) with a resonant frequency of ~300 kHz. The suspended atomically thin hBN sheets were mechanically exfoliated onto the substrate from hBN single crystals. The microwells with a depth of 2 μm in the 75 nm SiO_2/Si wafer were fabricated by photolithography. An Olympus BX51 optical microscope was used to locate suspended hBN sheets with preferable thicknesses. A multichip QCL (Daylight) was used for single-wavenumber s-SNOM imaging, and a tunable broadband laser (670 to 4000 cm^{-1}, 2.5 to 15 μm, Carmina APE) based on femtosecond optical parametric oscillator (OPO)/difference frequency generation (DFG) was used for scattering-type nanoIR spectroscopy. As illustrated in Figure S12, for both s-SNOM imaging and scattering-type nanoIR spectroscopy, the QCL/Camina IR laser source was incident on the 50/50 beamsplitter of an asymmetric Michelson interferometer. One arm is focused onto the AFM probe apex with a 90-degree off-axis parabolic mirror. Near-field tip−sample scattering light travels back along this sample arm, reflects off the beamsplitter, and interferometrically combines with retro-reflected light from a movable reference mirror at a mercury−cadmium−telluride detector. The AFM probe is dithered at ~300 kHz, and the near-field portion from tip−sample scattering is demodulated using a lock-in amplifier at higher harmonics of the tip oscillating frequency. In s-SNOM imaging, the second- or third-order demodulated optical signal was recorded at each pixel of the image, while in scattering-type nanoIR spectroscopy, the second-order demodulated signal was recorded as an interferogram, which was subsequently Fourier transformed into the spectrum. The acquisition of each interferogram took 3 min, and the spectral resolution is 2 cm^{-1}. OriginPro 9 was used for Gaussian peak fitting of the near-field amplitude spectra.

ASSOCIATED CONTENT

ⓢ Supporting Information
The Supporting Information is available free of charge at https://pubs.acs.org/doi/10.1021/acsnano.9b08895.

Real-space s-SNOM imaging of a 1.3 nm suspended hBN sheet, detailed peak-fitting analysis of the near-field amplitude spectra obtained from scattering-type nanoIR spectroscopy, comparison of near-field amplitude and phase spectra from half-suspended and nearly quarterly suspended regions, and near-field spectra taken from an hBN sample on the 300 nm SiO_2 substrate (PDF)

AUTHOR INFORMATION

Corresponding Author
*E-mail: k.kalantar-zadeh@unsw.edu.au.

ORCID ⓘ
Jiong Yang: 0000-0002-4367-5281
Mohammad B. Ghasemian: 0000-0002-5618-0106
Qingdong Ou: 0000-0003-2161-2543
Lu Hua Li: 0000-0003-2435-5220
Qiaoliang Bao: 0000-0002-6971-789X

Kourosh Kalantar-Zadeh: 0000-0001-6109-132X

REFERENCES

(1) Huth, F.; Govyadinov, A.; Amarie, S.; Nuansing, W.; Keilmann, F.; Hillenbrand, R. Nano-FTIR Absorption Spectroscopy of Molecular Fingerprints at 20 nm Spatial Resolution. *Nano Lett.* **2012**, *12*, 3973–3978.

(2) Xu, X. G.; Rang, M.; Craig, I. M.; Raschke, M. B. Pushing the Sample-Size Limit of Infrared Vibrational Nanospectroscopy: From Monolayer toward Single Molecule Sensitivity. *J. Phys. Chem. Lett.* **2012**, *3*, 1836–1841.

(3) Centrone, A. Infrared Imaging and Spectroscopy Beyond the Diffraction Limit. *Annu. Rev. Anal. Chem.* **2015**, *8*, 101–126.

(4) Mastel, S.; Govyadinov, A. A.; de Oliveira, T. V. A. G.; Amenabar, I.; Hillenbrand, R. Nanoscale-Resolved Chemical Identification of Thin Organic Films Using Infrared Near-Field Spectroscopy and Standard Fourier Transform Infrared References. *Appl. Phys. Lett.* **2015**, *106*, No. 023113.

(5) Amenabar, I.; Poly, S.; Nuansing, W.; Hubrich, E. H.; Govyadinov, A. A.; Huth, F.; Krutokhvostov, R.; Zhang, L.; Knez, M.; Heberle, J.; Bittner, A. M.; Hillenbrand, R. Structural Analysis and Mapping of Individual Protein Complexes by Infrared Nanospectroscopy. *Nat. Commun.* **2013**, *4*, 2890.

(6) Lyu, B.; Li, H.; Jiang, L.; Shan, W.; Hu, C.; Deng, A.; Ying, Z.; Wang, L.; Zhang, Y.; Bechtel, H. A.; Martin, M. C.; Taniguchi, T.; Watanabe, K.; Luo, W.; Wang, F.; Shi, Z. Phonon Polariton-Assisted Infrared Nanoimaging of Local Strain in Hexagonal Boron Nitride. *Nano Lett.* **2019**, *19*, 1982–1989.

(7) Bensmann, S.; Gaußmann, F.; Lewin, M.; Wüppen, J.; Nyga, S.; Janzen, C.; Jungbluth, B.; Taubner, T. Near-Field Imaging and Spectroscopy of Locally Strained GaN Using an IR Broadband Laser. *Opt. Express* **2014**, *22*, 22369–22381.

(8) Lucas, I. T.; McLeod, A. S.; Syzdek, J. S.; Middlemiss, D. S.; Grey, C. P.; Basov, D. N.; Kostecki, R. IR Near-Field Spectroscopy and Imaging of Single Li_xFePO_4 Microcrystals. *Nano Lett.* **2015**, *15*, 1–7.

(9) Amarie, S.; Zaslansky, P.; Kajihara, Y.; Griesshaber, E.; Schmahl, W. W.; Keilmann, F. Nano-FTIR Chemical Mapping of Minerals in Biological Materials. *Beilstein J. Nanotechnol.* **2012**, *3*, 312–323.

(10) Johnson, C. M.; Böhmler, M. Nano-FTIR Microscopy and Spectroscopy Studies of Atmospheric Corrosion with a Spatial Resolution of 20 nm. *Corros. Sci.* **2016**, *108*, 60–65.

(11) Amarie, S.; Ganz, T.; Keilmann, F. Mid-Infrared Near-Field Spectroscopy. *Opt. Express* **2009**, *17*, 21794–21801.

(12) Alfaro-Mozaz, F. J.; Alonso-González, P.; Vélez, S.; Dolado, I.; Autore, M.; Mastel, S.; Casanova, F.; Hueso, L. E.; Li, P.; Nikitin, A. Y.; Hillenbrand, R. Nanoimaging of Resonating Hyperbolic Polaritons in Linear Boron Nitride Antennas. *Nat. Commun.* **2017**, *8*, 15624.

(13) Autore, M.; Li, P.; Dolado, I.; Alfaro-Mozaz, F. J.; Esteban, R.; Atxabal, A.; Casanova, F.; Hueso, L. E.; Alonso-González, P.; Aizpurua, J.; Nikitin, A. Y.; Vélez, S.; Hillenbrand, R. Boron Nitride Nanoresonators for Phonon-Enhanced Molecular Vibrational Spectroscopy at the Strong Coupling Limit. *Light: Sci. Appl.* **2018**, *7*, 17172–17172.

(14) Ciano, C.; Giliberti, V.; Ortolani, M.; Baldassarre, L. Observation of Phonon-Polaritons in Thin Flakes of Hexagonal Boron Nitride on Gold. *Appl. Phys. Lett.* **2018**, *112*, 153101.

(15) Shi, Z.; Bechtel, H. A.; Berweger, S.; Sun, Y.; Zeng, B.; Jin, C.; Chang, H.; Martin, M. C.; Raschke, M. B.; Wang, F. Amplitude- and Phase-Resolved Nanospectral Imaging of Phonon Polaritons in Hexagonal Boron Nitride. *ACS Photonics* **2015**, *2*, 790–796.

(16) Dai, S.; Fei, Z.; Ma, Q.; Rodin, A.; Wagner, M.; McLeod, A.; Liu, M.; Gannett, W.; Regan, W.; Watanabe, K.; Taniguchi, T.; Thiemens, M.; Dominguez, G.; Castro Neto, A. H.; Zettl, A.; Keilmann, F.; Jarillo-Herrero, P.; Fogler, M. M.; Basov, D. N. Tunable Phonon Polaritons in Atomically Thin van der Waals Crystals of Boron Nitride. *Science* **2014**, *343*, 1125–1129.

(17) Ma, W.; Alonso-González, P.; Li, S.; Nikitin, A. Y.; Yuan, J.; Martín-Sánchez, J.; Taboada-Gutiérrez, J.; Amenabar, I.; Li, P.; Vélez, S.; Tollan, C.; Dai, Z.; Zhang, Y.; Sriram, S.; Kalantar-Zadeh, K.; Lee, S.-T.; Hillenbrand, R.; Bao, Q. In-Plane Anisotropic and Ultra-Low-Loss Polaritons in a Natural van der Waals Crystal. *Nature* **2018**, *562*, 557–562.

(18) Ambrosio, A.; Tamagnone, M.; Chaudhary, K.; Jauregui, L. A.; Kim, P.; Wilson, W. L.; Capasso, F. Selective Excitation and Imaging of Ultraslow Phonon Polaritons in Thin Hexagonal Boron Nitride Crystals. *Light: Sci. Appl.* **2018**, *7*, 27.

(19) Fali, A.; White, S. T.; Folland, T. G.; He, M.; Aghamiri, N. A.; Liu, S.; Edgar, J. H.; Caldwell, J. D.; Haglund, R. F.; Abate, Y. Refractive Index-Based Control of Hyperbolic Phonon-Polariton Propagation. *Nano Lett.* **2019**, *19*, 7725–7734.

(20) Giles, A. J.; Dai, S.; Vurgaftman, I.; Hoffman, T.; Liu, S.; Lindsay, L.; Ellis, C. T.; Assefa, N.; Chatzakis, I.; Reinecke, T. L.; Tischler, J. G.; Fogler, M. M.; Edgar, J. H.; Basov, D. N.; Caldwell, J. D. Ultralow-Loss Polaritons in Isotopically Pure Boron Nitride. *Nat. Mater.* **2018**, *17*, 134.

(21) Yoxall, E.; Schnell, M.; Nikitin, A. Y.; Txoperena, O.; Woessner, A.; Lundeberg, M. B.; Casanova, F.; Hueso, L. E.; Koppens, F. H. L.; Hillenbrand, R. Direct Observation of Ultraslow Hyperbolic Polariton Propagation with Negative Phase Velocity. *Nat. Photonics* **2015**, *9*, 674.

(22) Xu, X. G.; Ghamsari, B. G.; Jiang, J.-H.; Gilburd, L.; Andreev, G. O.; Zhi, C.; Bando, Y.; Golberg, D.; Berini, P.; Walker, G. C. One-Dimensional Surface Phonon Polaritons in Boron Nitride Nanotubes. *Nat. Commun.* **2014**, *5*, 4782.

(23) Kumar, A.; Low, T.; Fung, K. H.; Avouris, P.; Fang, N. X. Tunable Light—Matter Interaction and the Role of Hyperbolicity in Graphene—hBN System. *Nano Lett.* **2015**, *15*, 3172–3180.

(24) Zhao, B.; Zhang, Z. M. Resonance Perfect Absorption by Exciting Hyperbolic Phonon Polaritons in 1D hBN Gratings. *Opt. Express* **2017**, *25*, 7791–7796.

(25) Tielrooij, K.-J.; Hesp, N. C.; Principi, A.; Lundeberg, M. B.; Pogna, E. A.; Banszerus, L.; Mics, Z.; Massicotte, M.; Schmidt, P.; Davydovskaya, D.; Purdie, D. G.; Goykhman, I.; Soavi, G.; Lombardo, A.; Watanabe, K.; Taniguchi, T.; Bonn, M.; Turchinovich, D.; Stampfer, C.; Ferrari, A. C.; et al. Out-of-Plane Heat Transfer in van der Waals Stacks Through Electron—Hyperbolic Phonon Coupling. *Nat. Nanotechnol.* **2018**, *13*, 41.

(26) Dai, S.; Ma, Q.; Andersen, T.; McLeod, A. S.; Fei, Z.; Liu, M. K.; Wagner, M.; Watanabe, K.; Taniguchi, T.; Thiemens, M.; Keilmann, F.; Jarillo-Herrero, P.; Fogler, M. M.; Basov, D. N. Subdiffractional Focusing and Guiding of Polaritonic Rays in a Natural Hyperbolic Material. *Nat. Commun.* **2015**, *6*, 6963.

(27) Dai, S.; Quan, J.; Hu, G.; Qiu, C.-W.; Tao, T. H.; Li, X.; Alù, A. Hyperbolic Phonon Polaritons in Suspended Hexagonal Boron Nitride. *Nano Lett.* **2019**, *19*, 1009–1014.

(28) Govyadinov, A. A.; Amenabar, I.; Huth, F.; Carney, P. S.; Hillenbrand, R. Quantitative Measurement of Local Infrared Absorption and Dielectric Function with Tip-Enhanced Near-Field Microscopy. *J. Phys. Chem. Lett.* **2013**, *4*, 1526–1531.

(29) Ambrosio, A.; Jauregui, L. A.; Dai, S.; Chaudhary, K.; Tamagnone, M.; Fogler, M. M.; Basov, D. N.; Capasso, F.; Kim, P.; Wilson, W. L. Mechanical Detection and Imaging of Hyperbolic Phonon Polaritons in Hexagonal Boron Nitride. *ACS Nano* **2017**, *11*, 8741−8746.

(30) Gilburd, L.; Kim, K. S.; Ho, K.; Trajanoski, D.; Maiti, A.; Halverson, D.; de Beer, S.; Walker, G. C. Hexagonal Boron Nitride Self-Launches Hyperbolic Phonon Polaritons. *J. Phys. Chem. Lett.* **2017**, *8*, 2158−2162.

(31) Dai, S.; Fang, W.; Rivera, N.; Stehle, Y.; Jiang, B.-Y.; Shen, J.; Tay, R. Y.; Ciccarino, C. J.; Ma, Q.; Rodan-Legrain, D.; Jarillo-Herrero, P.; Teo, E. H. T.; Fogler, M. M.; Narang, P.; Kong, J.; Basov, D. N. Phonon Polaritons in Monolayers of Hexagonal Boron Nitride. *Adv. Mater.* **2019**, *31*, 1806603.

(32) Zhang, L. M.; Andreev, G. O.; Fei, Z.; McLeod, A. S.; Dominguez, G.; Thiemens, M.; Castro-Neto, A. H.; Basov, D. N.; Fogler, M. M. Near-Field Spectroscopy of Silicon Dioxide Thin Films. *Phys. Rev. B: Condens. Matter Mater. Phys.* **2012**, *85*, No. 075419.

(33) Li, S.-L.; Miyazaki, H.; Song, H.; Kuramochi, H.; Nakaharai, S.; Tsukagoshi, K. Quantitative Raman Spectrum and Reliable Thickness Identification for Atomic Layers on Insulating Substrates. *ACS Nano* **2012**, *6*, 7381−7388.

(34) Wang, Y. Y.; Ni, Z. H.; Shen, Z. X.; Wang, H. M.; Wu, Y. H. Interference Enhancement of Raman Signal of Graphene. *Appl. Phys. Lett.* **2008**, *92*, No. 043121.

(35) Yang, J.; Wang, Z.; Wang, F.; Xu, R.; Tao, J.; Zhang, S.; Qin, Q.; Luther-Davies, B.; Jagadish, C.; Yu, Z.; Lu, Y. Atomically Thin Optical Lenses and Gratings. *Light: Sci. Appl.* **2016**, *5*, No. e16046.